

1 **Title:** Scaling of G1 duration with population doubling time by a cyclin in *Saccharomyces*
2 *cerevisiae*

3

4 **Authors:** Heidi M. Blank^{*}, Michelle Callahan^{*}, Ioannis P.E. Pistikopoulos^{*}, Aggeliki O. Polymenis^{**}
5 and Michael Polymenis^{*}

6

7 **Affiliations:** ^{*}Department of Biochemistry and Biophysics, Texas A&M University, College Station, TX
8 77843, U.S.A.

9 [†]Present address: Department of Physics and Astronomy, University of California, Los
10 Angeles, CA 90095

11 **Running Title:** Scaling G1 with doubling time

12 **Keywords:** cell size / growth law / START / chemostat

13 **Correspondence:** Heidi M. Blank or Michael Polymenis

14 Department of Biochemistry and Biophysics, Texas A&M University

15 300 Olsen Blvd., College Station, TX, 77843-2128

16 HeidiBlank@tamu.edu (H.M.B); polymenis@tamu.edu (M.P.)

17 Tel: 979-458-3259

18 **ABSTRACT**

19 The longer cells stay in particular phases of the cell cycle, the longer it will take these cell populations to
20 increase. However, the above qualitative description has very little predictive value, unless it can be
21 codified mathematically. A quantitative relation that defines the population doubling time (T_d) as a
22 function of the time eukaryotic cells spend in specific cell cycle phases would be instrumental for
23 estimating rates of cell proliferation and for evaluating introduced perturbations. Here, we show that in
24 human cells the length of the G1 phase (T_{G1}) regressed on T_d with a slope of ≈ 0.75 , while in the yeast
25 *Saccharomyces cerevisiae* the slope was slightly smaller, at ≈ 0.60 . On the other hand, cell size was not
26 strongly associated with T_d or T_{G1} in cell cultures that were proliferating at different rates. Furthermore,
27 we show that levels of the yeast G1 cyclin Cln3p were positively associated with rates of cell
28 proliferation over a broad range, at least in part through translational control mediated by a short uORF
29 in the *CLN3* transcript. Cln3p was also necessary for the proper scaling between T_{G1} and T_d . In contrast,
30 yeast lacking the Whi5p transcriptional repressor maintained the scaling between T_{G1} and T_d . These data
31 reveal fundamental scaling relations between the duration of eukaryotic cell cycle phases and rates of
32 cell proliferation, point to the necessary role of Cln3p in these relations in yeast and provide a
33 mechanistic basis linking Cln3p levels to proliferation rates and the scaling of G1 with doubling time.

34 INTRODUCTION

35 Recurring shapes and patterns in nature are sometimes described with mathematical relationships. As a
36 result, these natural processes can be predicted and understood better. Regarding patterns of
37 eukaryotic cell division, one could ask: How are the lengths of eukaryotic cell cycle phases related to
38 each other and to the total doubling time of the population? Can such relations be described
39 mathematically, in the form of a scaling formula? If so, what are the molecular mechanisms that govern
40 the scaling? A scaling relation that describes eukaryotic cell division would be a significant advance. For
41 example, it could serve as a point of reference against which the effects of genetic or other
42 perturbations can be evaluated.

43 The 'textbook' view in the coordination of growth and division in the eukaryotic cell cycle (e.g., see
44 Fig. 10-26 in (MORGAN 2007)) is that expansion of the G1 phase of the eukaryotic cell cycle accounts for
45 most, if not all, of the lengthening of the cell cycle in slower proliferating cells, in budding yeast
46 (JOHNSTON *et al.* 1977; BRAUER *et al.* 2008) or humans (BASERGA 1985; FISHER 2016). However, there is no
47 report in the literature of a quantitative relation that defines the doubling time (T_d) as a function of the
48 time yeast or human cells spend in the G1 phase (T_{G1}). Here, based on all the available data for budding
49 yeast and human cell populations, we derived for the first time in the field scaling relations between T_{G1}
50 and T_d . These scaling relations also allowed us to critically evaluate the role of cell cycle regulators in
51 yeast cells proliferating at different rates.

52 Two key regulators of the length of the G1 phase in *S. cerevisiae* are the Cln3p and Whi5p proteins.
53 The G1 cyclin Cln3p promotes initiation of DNA replication (CROSS 1988; NASH *et al.* 1988). In contrast,
54 the transcriptional repressor Whi5p acts analogously to the retinoblastoma gene product in animals, to
55 inhibit the G1/S transition (COSTANZO *et al.* 2004; DE BRUIN *et al.* 2004; PALUMBO *et al.* 2016). It has been
56 reported that while synthesis of Cln3p parallels cell size, the synthesis of Whi5p is independent of cell

57 size (SCHMOLLER *et al.* 2015), arguing that dilution of Whi5p as cells get bigger in G1 governs the length of
58 the G1 phase (SCHMOLLER AND SKOTHEIM 2015; SCHMOLLER *et al.* 2015).

59 Here, we obtained the first measurements of Cln3p and Whi5p levels as a function of proliferation
60 rates in steady-state cultures. The levels of Cln3p varied over a broad range, due to a uORF affecting
61 translation of *CLN3*. Our data also show that loss of Whi5p does not significantly affect the scaling
62 relation between T_d and T_{G1} . Instead, we provide strong evidence for the functional and molecular basis
63 for the necessary role of Cln3p in this process.

64 MATERIALS AND METHODS

65 **Strains.** Unless stated otherwise, *S. cerevisiae* wild-type, *cln3Δ* and *whi5Δ* strains were in the BY4741
66 background (NCBI Taxon 559292; *MATa*, *his3Δ1*, *leu2Δ0*, *ura3Δ0*, *met15Δ0*) and they have been
67 described previously (SOMA *et al.* 2014). For protein surveillance, we constructed an otherwise wild type
68 strain that carried epitope-tagged *WHI5* and *CLN3* alleles at their endogenous chromosome locations.
69 First, a commercially available *WHI5-TAP::HIS3* strain (BY4741 otherwise; GE Healthcare) was
70 backcrossed three times into the W303 background (NCBI Taxon 580240; *MATa leu2-3,112 trp1-1 can1-*
71 *100 ura3-1 ade2-1 his3-11,15*). Then, it was crossed with an otherwise wild-type strain carrying a *CLN3-*
72 *13MYC* allele (W303 background) described elsewhere (THORBURN *et al.* 2013), and kindly provided by
73 Dr. A. Amon (MIT and HHMI). The resulting diploid was sporulated and dissected, to obtain *MATa*
74 haploid segregants carrying both the epitope-tagged *WHI5* and *CLN3* alleles (strains HB94/97; *MATa*
75 *CLN3-13MYC::TRP⁺ WHI5-TAP::HIS⁺ leu2 ura3 met15*), which were used in the experiments shown in
76 Figure 4. We verified expression of Whi5p-TAP and Cln3p-(Myc)₁₃ in this strain (see Supplementary File
77 1), and their absence in *whi5Δ* or *cln3Δ* strains, respectively. We also generated a derivative of this
78 strain, which lacks the uORF in the 5'-leader of the *CLN3* mRNA. To this end, we used plasmid A-315T-
79 pMT10 we had described previously (POLYMENIS AND SCHMIDT 1997), as a template in a PCR reaction with
80 forward (5'-CAAGAACTACCATTCGACAGG-3') and reverse primers (5'-CGTACAGAAAGCGTATCAAA-3') to
81 generate a product that carries in the 5'-leader of *CLN3* the *URA3*-marked A-315T mutation that
82 inactivates the uORF. We then used this PCR product to transform strain HB94 (*WHI5-TAP*, *CLN3-*
83 *13MYC*). Genomic DNA of transformants was sequenced to verify the presence of the A-315T mutation.
84 Confirmed A-315T mutants were then backcrossed with wild type (W303) to segregate away possible
85 secondary mutations at other loci. The resulting heterozygote was sporulated and dissected to isolate a
86 *WHI5-TAP*, *A-315T-CLN3-13MYC* segregant (HB104), which was used in the experiments shown in Figure
87 4.

88

89 **Datasets for population-based cell cycle parameters.** All the obtained variables we report here
90 represent population averages. They do not resolve intergenerational differences in cell cycle
91 progression of the same cells in successive cell cycles. In the context of this study, population averages
92 hold significant advantages: First, they are easily obtained; Second, they are ubiquitously used and
93 reported in the literature; Third, they allow straightforward comparisons between different systems, for
94 example between yeast and human cells (see Figure 1).

95 For yeast, the data we collected (Table S1) were from wild type strains from various backgrounds,
96 except in the few cases where they carried temperature-sensitive alleles, such as *cdc* mutations
97 (JAGADISH AND CARTER 1977), to estimate the length of the G1 phase upon transfer to the non-permissive
98 temperature. The methods used to calculate the fraction of G1 cells included: measurements of the DNA
99 content of the cells by flow cytometry (SLATER *et al.* 1977; JOHNSTON *et al.* 1980; GUO *et al.* 2004; BRAUER
100 *et al.* 2008; HENRY *et al.* 2010); budding (TYSON *et al.* 1979; RIVIN AND FANGMAN 1980); sensitivity to cell
101 cycle arrest before DNA replication by pheromone (HARTWELL AND UNGER 1977; JAGADISH AND CARTER
102 1977), or *cdc* (JAGADISH AND CARTER 1977) mutations. In this study, to obtain the fraction of G1 cells (e.g.,
103 see Figures 3, 4), we used DNA content measurements by flow cytometry, as described previously
104 (HOOSE *et al.* 2012; HOOSE *et al.* 2013).

105 For human cells, earlier studies employed ³H-thymidine pulses or division waves after thymidine
106 block (BASERGA 1985). The doubling times of the NCI-60 human cancer cell lines we included in Table S2
107 are known (ROSS *et al.* 2000; SCHERF *et al.* 2000; POLYMENIS 2017), but there was no quantitative cell cycle
108 data for most of the cell lines. However, images of DNA content profiles for the NCI-60 panel, albeit with
109 no quantification, have been published (GARNER AND EASTMAN 2011). We requested and obtained high-
110 resolution files of these images from Dr. Alan Eastman (Geisel School of Medicine - Dartmouth College).

111 From the entire DNA content histogram, to quantify the fraction of cells in G1, we used imaging
112 software to measure the area on the left side of the G1 peak (from peak to valley) and multiplied this
113 area by two, as has been described previously (JOHNSTON *et al.* 1980). This approach avoids
114 complications from heavy right side tails due to S phase cells and yields an acceptable estimate of the
115 relative G1 length as a fraction of total cell cycle time. We then combined these values with all others
116 available from human cells, cancerous and normal (SISKEN AND KINOSITA 1961; DEFENDI AND MANSON 1963;
117 LENNARTZ AND MAURER 1964; AOKI AND MOORE 1970; BASERGA 1985; KUMEI *et al.* 1989; BRONS *et al.* 1992;
118 LUCIANI *et al.* 2001; HAHN *et al.* 2009), to compile a dataset of 96 values for G1 length (T_{G1}) and doubling
119 time (T_d) for human cells, shown in Table S2.

120

121 **Estimates of G1 length.** The values we show in Tables S1 and S2 were obtained from studies reporting
122 on the *relative* duration of the G1 phase. To estimate the *absolute* length of the G1 phase, T_{G1} , we
123 multiplied the relative G1 length by T_d (Tables S1, S2). This simple equation is the appropriate one to use
124 with chemostat data when as many cells are removed as are being produced in the culture (HOFFMAN
125 1949). Subtracting T_{G1} from T_d yields the duration of the rest of the cell cycle phases (T_{nonG1}). For non-
126 chemostat data, other more elaborate equations could be used, especially for the asymmetric patterns
127 of division of budding yeast (HARTWELL AND UNGER 1977; JOHNSTON *et al.* 1980). However, for simplicity
128 and ease of comparison across systems, we uniformly applied the simple equation mentioned above.
129 Furthermore, inaccuracies in the absolute values of T_{G1} may only affect the intercept of the linear
130 relation between T_d and T_{G1} , but not the slope that describes the fundamental scaling between T_d and
131 T_{G1} , or any of our conclusions. Indeed, when we plotted in the same manner as in Figure 1 only the
132 chemostat values in Table S1 (94 data points), the slope of $\ln T_d \propto \ln T_{G1}$ was 0.6107. For the remaining,
133 non-chemostat values (55 data points), the slope of $\ln T_d \propto \ln T_{G1}$ was 0.6074.

134 Lastly, a limitation of the non-chemostat data in yeast and all the data from human cells is that it is
135 assumed that cell death contributes negligibly to the doubling time of the population. This assumption is
136 reasonable in yeast because young cells vastly outnumber older ones approaching senescence.
137 However, it may be of concern in mammalian culture systems. Hence, our data with human cells should
138 be interpreted with caution, because the fraction of growing cells in the culture may be significantly
139 lower than one. Also, although we are looking at trends that seemingly hold across a multitude of
140 human cell types, the data were overwhelmingly derived from cancer cell lines, which in many cases
141 have altered cell cycles.

142

143 **Chemostat cultures.** The experiments were done using a New Brunswick BioFlo (BF-110) reactor with a
144 working volume of 880 mL. The reactor was run at room temperature, as described earlier (HENRY *et al.*
145 2010). In each experiment and at each dilution rate the reactor was sampled several times to measure
146 protein levels by immunoblots, the DNA content with flow cytometry, and the cell size and cell density
147 of the culture using a Beckman Z2 channelyzer (HENRY *et al.* 2010; HOOSE *et al.* 2012), as indicated. We
148 measured the cell density at every sampling, to ensure that we never reached ‘wash-out’ conditions at
149 the high dilution rates. In every experiment the cell density remained $>1E+07$ cells/ml and did not vary
150 more than 3-fold between the lowest and highest dilution rates.

151

152 **Protein surveillance.** Proteins were resolved onto 4-12% Tris-Glycine gels (Thermo Scientific, Cat#: XP04125BOX). Cln3p-(Myc)₁₃ was detected with an anti-Myc antibody (Abcam, Cat #: ab13836). All other
153 procedures for TAP-tagged protein detection, extract preparation for immunoblots and their analysis
154 have been described elsewhere (BLANK *et al.* 2017).

156

157 **Statistical analysis.** Data were analyzed and displayed with R language packages. All R functions, the
158 corresponding packages, and their use are listed in Table S3. To build the linear models we described
159 using the values for the yeast (Table S1) and human (Table S2) datasets, we first examined if the
160 assumptions for building simple, linear parametric models were satisfied. The diagnostic residual plots
161 evaluating whether the errors were independent of each other, normally distributed around a mean of
162 zero and equal variance, are shown in Figure S2. In both the yeast and human datasets, the existence of
163 a few outlier points appeared to violate the necessary assumptions (Figure S2; $p < 0.05$ for assessment of
164 the assumptions using the global test on four degrees-of-freedom (PENA AND SLATE 2006)). Hence, we
165 opted for non-parametric, robust linear regression models based on Siegel repeated medians (Table 1).
166 For the meta-analysis of cell size data (see Figure 2) we used the *metafor* R language package
167 (VIECHTBAUER 2010). Briefly, the correlation coefficients from each study were transformed using Fisher's
168 z transformation. An unbiased random-effects analysis, as opposed to a fixed-effects one, was then
169 performed using this index, and the summary values were converted back to correlations and displayed
170 as such with forest plots (Figure 2, Table S3).

171

172 **Data availability.** Strains and plasmids are available upon request. The authors affirm that all data
173 necessary for confirming the conclusions of the article are present within the article, figures, and tables.
174 Figure S1 shows goodness-of-fit plots for lognormal distribution of yeast and human T_{G1} values. Figure
175 S2 shows diagnostic plots of simple linear regression models for T_d and T_{G1} values of yeast and human
176 cells. Figure S3 shows additional chemostat experiments with *whi5Δ* and *cln3Δ* cells. Table S1 lists all the
177 cell cycle values for yeast cells from the literature. Table S2 lists all the cell cycle values for human cells
178 from the literature. Table S3 lists all R functions, the corresponding packages, and their use. File S1
179 contains all raw immunoblot images generated and used in this study. All supplementary figures, tables
180 and files can be found at ([10.6084/m9.figshare.7011275](https://doi.org/10.6084/m9.figshare.7011275)).

181 RESULTS

182 Rationale

183 The rationale for the experiments we describe was the following: First, use all the available values from
184 the literature to derive a quantitative relationship of the population doubling time (T_d) as a function of
185 the time eukaryotic cells spend in the G1 phase of the cell cycle (T_{G1}) (Figure 1). Second, based on the
186 same datasets and analyses, examine if cell size is also related to T_d or T_{G1} , because cell size is often used
187 as a proxy for the control of cell division by nutrients (Figure 2). Third, use the linear relation linking T_d
188 and T_{G1} as a metric to evaluate the contributions of Whi5p and Cln3p, two proteins that govern the G1/S
189 transition in budding yeast (Figure 3). Fourth, if Cln3p or Whi5p impinges on the relation between T_d
190 and T_{G1} , then provide a mechanistic understanding of its role (Figure 4).

191

192 T_{G1} values are distributed lognormally, consistent with exponential patterns of growth

193 We compiled the available values for T_d and T_{G1} from the literature for budding yeast (Table S1) and
194 human (Table S2) cells (see Materials and Methods). With the dataset of T_{G1} values at hand, we next
195 examined their distribution. Knowing how the T_{G1} values are distributed will inform how to better model
196 T_{G1} against T_d and offer some insight into the processes that determine G1 length. We found that T_{G1}
197 values were not normally distributed for yeast ($p = 4.434E-14$, Shapiro-Wilk test) or human cells ($p =$
198 $1.039E-07$, Shapiro-Wilk test). Instead, T_{G1} values fit better a lognormal distribution. For example, for
199 yeast T_{G1} values, the Anderson-Darling statistic was the lowest for the lognormal distribution (0.347),
200 compared to other distributions (Weibull: 1.693; gamma: 1.521; exponential: 2.462). As expected for
201 lognormal distributions, log-transformed values of T_{G1} were normally distributed for yeast (Figure S1A-D,
202 $p = 0.1871$, Shapiro-Wilk test) and human cells (Figure S1E-H, $p = 0.3099$, Shapiro-Wilk test). The
203 apparent lognormal distribution of T_{G1} values is consistent with a multiplicative process of many,

204 positive, independent random variables that determine the G1 length (KOCH 1966). Lognormal
205 distributions are very common in biological growth processes (MOSIMANN 1988). In cell proliferation,
206 lognormality has been proposed to reflect exponential patterns of growth in mass. Despite fluctuations
207 in the growth rate constant, the growth of the overwhelming majority of cellular components is
208 influenced similarly, leading to lognormality (KOCH AND SCHAECHTER 1962; KOCH 1966). In budding yeast
209 and other cell types there is evidence for exponential patterns of protein synthesis (ELLIOTT AND
210 MCLAUGHLIN 1978; DI TALIA *et al.* 2007; TZUR *et al.* 2009) and increase in mass in the cell cycle (BRYAN *et al.*
211 2012; SON *et al.* 2012). Such considerations accommodate the lognormality of T_{G1} values we describe
212 here.

213

214 **Strong association between T_{G1} and T_d , but non-G1 phases also expand in lower proliferation rates**

215 To test for association between T_{G1} and T_d we used the distribution-free Spearman's and Kendall's tests
216 for independence based on ranks. We used these non-parametric, distribution-free tests because of the
217 existence of outliers even in log-transformed T_{G1} values (e.g., see Figure S1). The high values (> 0.75) of
218 the rank correlation coefficients (τ for Kendall's and r for Spearman's; see Table 1) show a strong
219 positive association between T_{G1} and T_d , for both yeast (Figure 1A) and human (Figure 1C) cells.
220 Interestingly, however, the duration of the non-G1 phases (T_{nonG1}) of the cell cycle were also positively
221 correlated with T_d (Figures 1B, D; and Table 1) in both organisms, albeit less so in yeast ($\tau=0.398$; Figure
222 1B) than in human cells ($\tau=0.579$; Figure 1D). Overall, our data document the strong association between
223 T_{G1} and T_d (Figures 1A, C). Additionally, they suggest that growth requirements for cell division are not
224 registered exclusively in G1, but also later in the cell cycle (see Figures 1B, D), in agreement with
225 observations from other groups (ANASTASIA *et al.* 2012; FERREZUELO *et al.* 2012; DOWLING *et al.* 2014;
226 SOIFER AND BARKAI 2014; CERULUS *et al.* 2016; MAYHEW *et al.* 2017; GARMENDIA-TORRES *et al.* 2018).

227 **A scaling relation between T_{G1} and T_d**

228 To estimate a predictive and quantitative relation between T_{G1} and T_d we derived non-parametric,
229 robust linear regression models using the Siegel repeated median estimates (SIEGEL 1982), (Figure 1 and
230 Table 1; see also Materials and Methods). The intercepts of the linear T_{G1} vs. T_d plots reflect the
231 apparent minimum duration of the S+G2+M phases in yeast (1.4 h; Table 1) and human (7.6 h; Table 1)
232 cells. The slopes in the linear relations indicate how much T_d is affected by T_{G1} , or T_{nonG1} . For example, if
233 non-G1 phases were not expanding in slower proliferating cells, then one would expect a vertical line
234 parallel to the y-axis in T_{nonG1} vs. T_d plots. We noticed that the slope of the regression of T_{G1} on T_d
235 appeared to slightly differ between the yeast and human datasets (Figure 1 and Table 1). Applying the
236 non-parametric Sen-Adichie test for parallelism confirmed that the difference in the slopes of the
237 regression lines of T_{G1} on T_d between yeast and human cells was statistically significant (V statistic =
238 7.324, p-value = 0.007). Although the T_{G1} distributions themselves are lognormal, log-transformation is
239 not necessary for any of our conclusions, since we used a non-parametric, ordinal-based analysis in all
240 our statistical tests. Nonetheless, we display regression plots using log-transformed data to improve
241 visualization, because data points appear more evenly on these graphs. Furthermore, log-transformed
242 values are often incorporated in scaling relations between the measured variables in the literature (CHAN
243 AND MARSHALL 2010). The quantitative relations we identified linking T_{G1} with T_d are significant because
244 they provide a framework to interpret experimental perturbations in cell cycle progression and cell
245 proliferation, as we will describe for yeast cells.

246

247 **Nutrient-specific, but not growth rate-dependent association between cell size and T_{G1} , or T_d .**

248 Control of cell size has frequently been used synonymously with growth control of G1 transit in the cell
249 cycle, especially in budding yeast. Daughter cells of *S. cerevisiae* are born smaller than their mother is,
250 and they will not initiate a new round of cell division until they reach a size characteristic of the culture

251 medium. The rate at which daughter cells increase in volume has been reported to contribute to the size
252 at which they will initiate a new round of cell division (FERREZUELO *et al.* 2012). Note that unless indicated
253 otherwise, here we use the term ‘growth rate’ to describe the rate at which cells proliferate, and not the
254 rate at which they increase in size in a given cell cycle. As the cell cycle is prolonged in poor nutrients, it
255 is also widely assumed that the cells get smaller (e.g., see Fig. 10-26 in (MORGAN 2007)). To test the
256 strength of the association between cell size and T_{G1} or T_d , we combined the available data from
257 previous studies ((TYSON *et al.* 1979; GUO *et al.* 2004; BRAUER *et al.* 2008); see Table S1). From such an
258 unbiased but unweighted analysis (Figure 2A, D), it appeared that the size of yeast cells was not
259 significantly associated with T_d (p-value= 0.171, based on Kendall’s test; Figure 2A) or T_{G1} (p-value=
260 0.2449, based on Kendall’s test; Figure 2D).

261 Unlike the strong association of T_{G1} with T_d , which was consistent across studies (see Figure 1 and
262 Materials and Methods), the association between cell size and T_{G1} or T_d appeared to vary among the
263 relevant studies. Given the different number of samples analyzed in each study and their associated
264 variance, we calculated the effect sizes from each study separately, based on the non-parametric
265 Spearman’s and Kendall’s correlation coefficients. These study-specific correlation coefficients then
266 served as the effect size index, to standardize the different studies and arrive at a summary correlation
267 (BORENSTEIN 2009). The results were visualized in typical ‘forest’ plots (Figures 2B, C, E, F). A negative
268 association between size and rates of cell proliferation, with cells getting smaller with larger T_d values,
269 was only evident at a moderate level in batch cultures ($\tau = -0.52$, $r = -0.64$; see Figures 2E, F), where
270 different nutrients were used to achieve different doubling times (TYSON *et al.* 1979). In contrast, in
271 other studies (GUO *et al.* 2004; BRAUER *et al.* 2008), which employed chemostats to alter the population
272 doubling time independently of the limiting nutrient, there was no correlation between cell size and T_d
273 or T_{G1} (Figure 2). Importantly, within these chemostat studies, cell size measurements were internally
274 calibrated. Hence, the lack of any correlation between cell size and T_d or T_{G1} cannot be attributed to

275 experimental variabilities of different studies incorporated in our meta-analysis of the literature. Lastly,
276 the lack of a significant association between T_{G1} and cell size agrees with a genome-wide survey of single
277 gene deletions (Hoose *et al.* 2012), which found no pattern of correlation between cell size and the
278 relative duration of the G1 phase. Hence, although cell size can be modulated by changes in nutrient
279 composition in yeast ((Tyson *et al.* 1979; SOMA *et al.* 2014); and others), our data suggest that it is more
280 likely that these are nutrient-specific effects, not causally linked to changes in cell proliferation rates.

281

282 **Cln3p, but not Whi5p, is required for the strong association between T_{G1} and T_d**

283 To understand how the relation between the length of the G1 phase and doubling time is established in
284 budding yeast, we next examined the role of the Cln3p and Whi5p proteins, which regulate the G1/S
285 transition in this organism. It has been proposed that dilution of Whi5p as cells get bigger in G1 is the
286 key event controlling the timing of the G1/S transition (SCHMOLLER AND SKOTHEIM 2015; SCHMOLLER *et al.*
287 2015). Since in cells proliferating at different rates there is not a significant correlation with cell size
288 (Figure 2, Table S1), it is not clear how the inhibitor dilution model would apply to the conditions we
289 examine in this study. To our knowledge, the kinetics of cell cycle progression in cells lacking Cln3p or
290 Whi5p have not been examined previously in steady-state cultures proliferating at different rates. To
291 test the role of Cln3p and Whi5p in the relation between T_{G1} and T_d , we examined the cell cycle profile
292 of *cln3Δ* or *whi5Δ* cells in continuous, steady-state chemostat cultures. We measured T_{G1} in *cln3Δ* or
293 *whi5Δ* cells from the DNA content of the cultures under glucose (0.08% w/v) limitation and at different
294 dilution rates (0.038 h^{-1} to 0.348 h^{-1} ; corresponding to T_d values between 18 h and 2 h, respectively). As
295 expected, cells lacking Whi5p were very small (≈ 18 fL), and their size did not change significantly as a
296 function of T_d (Figures 3E and S3D). Furthermore, the intercept of the linear fit between the log-
297 transformed T_d and T_{G1} values of *whi5Δ* cells was significantly higher than the intercept of the linear fit
298 of these parameters in wild-type cells (1.17 vs. 0.92; see Table 1), consistent with the shortened G1

299 phase of *whi5Δ* cells. The slope of the linear relation between T_d and T_{G1} in *whi5Δ* cells (Figure 3B) was
300 similar to what we observed in the aggregate analysis of wild-type cells (Figure 1A, and Table 1; Sen-
301 Adichie V statistic = 1.775, p-value = 0.183), albeit slightly smaller than the slope of wild type cells from a
302 separate, independent experiment performed in this study (0.6723 in wild type (Fig. 3A) vs. 0.6166 in
303 *whi5Δ* cells (Fig. 3B)). These data suggest that in different physiological states, and despite their
304 shortened G1 phase and small size, *whi5Δ* cells nonetheless remain responsive to different
305 environments, displaying minimal changes in their scaling of the expected proportional changes
306 between T_d and T_{G1} .

307 In contrast, cells lacking Cln3p had an abnormal behavior. In three independent experiments
308 (Figures 3C, and S3B,C), T_{G1} did not even have a straightforward linear relation with T_d in cultures of
309 *cln3Δ* cells. At shorter division times ($T_d < 5$ h), the T_d and T_{G1} values of *cln3Δ* cultures were related
310 linearly, albeit with a higher slope (e.g., Figure S3C; slope = 0.7685). More importantly, in all three
311 independent experiments, the linear relation breaks down at slower proliferating *cln3Δ* cultures (Figures
312 3C, and S3B,C). Even when combining all data points from the individual experiments for each strain, we
313 found that at all doubling times tested the linear relation between T_d and T_{G1} remains strong for *whi5Δ*
314 cells ($\tau > 0.8$, based on Kendall's non-parametric test). The same is true for *cln3Δ* cells at values of $\text{Ln}T_d <$
315 1.5 (corresponding to T_d values < 4.5 h). In contrast, the linear relation between T_d and T_{G1} is significantly
316 weaker ($\tau < 0.5$) for slower proliferating *cln3Δ* cells ($\text{Ln}T_d > 1.5$). These data suggest that Cln3p is more
317 important than Whi5p for imposing the proper scaling relation of $T_d \propto T_{G1}$ in wild type cells.

318

319 **Cln3p levels are strongly and positively associated with cell proliferation rates**

320 Given the important role of Cln3p in establishing the proper relation between T_d and T_{G1} (Figures 3 and
321 S3), we sought to measure the levels of Cln3p and Whi5p as a function of T_d . There are no reports of the
322 steady-state levels of Cln3p or Whi5p in cell populations proliferating at different rates in chemostats.

323 To measure Whi5p and Cln3p levels from the same cells, we generated a strain that carries *WHI5-TAP*
324 and *CLN3-13MYC* alleles, providing the only source of these gene products in the cells, expressed from
325 their endogenous chromosomal locations (Figure 4A, see Materials and Methods). The expressed
326 proteins were epitope-tagged, but otherwise un-mutated, wild type Whi5p-TAP and Cln3p-(Myc)₁₃.
327 These cells were then cultured in continuous, steady-state chemostat cultures under glucose (0.08% w/v)
328 or leucine (0.0015% w/v) limitation. Although the *CLN3-13MYC* allele provides the means for reliable
329 detection of otherwise wild type Cln3p, it is known to be slightly hypermorphic, stabilizing the Cln3p
330 protein somewhat and shortening the G1 phase of the cell cycle (THORBURN *et al.* 2013). Indeed, the
331 intercept of the linear fit between the log-transformed T_d and T_{G1} values of this strain (HB94; *WHI5-TAP*,
332 *CLN3-13MYC*) was slightly higher than the intercept of the linear fit of these parameters in wild-type
333 cells (0.97 vs. 0.92; see Table 1), consistent with a shortened G1 phase. The slope of the linear relation
334 between the log-transformed values of T_d and T_{G1} was increased somewhat for these cells compared to
335 the aggregate analysis of wild-type cells (0.68 vs. 0.6; see Table 1). Importantly, these cells still displayed
336 a strong, linear, positive association between T_d and T_{G1} ($\tau=0.77$; $r=0.92$; see Table 1), at all dilution rates
337 we tested. Hence, we concluded that the relation between T_d and T_{G1} was only minimally affected in this
338 strain, and we proceeded to quantify the levels of both Whi5p-TAP and Cln3p-(Myc)₁₃, from separate
339 chemostat experiments under glucose or leucine limitation, each run at ≥ 5 dilution rates (Figure 4; see
340 Materials and Methods).

341 The levels of Whi5p-TAP were not increased in slower proliferating cells (Figure 4A, B). Previously,
342 (LIU *et al.* 2015) reported that Whi5p abundance increases ≈ 3 -fold in cells growing in poorer carbon
343 sources, although this was not seen in a more recent study by (DORSEY *et al.* 2018). In any case, several
344 variables were different between the (LIU *et al.* 2015) study and ours, which could account for the
345 disagreement in the findings: First, different epitope-tagged alleles were used (*WHI5-tdTomato* vs.
346 *WHI5-TAP*). Second, different detection methods were applied (fluorescence live cell imaging vs.

347 immunoblots). Third, (LIU *et al.* 2015) use cells in the W303 background, which are larger than cells of
348 the BY background we use here, possibly leading to differences in cell size regulation. Fourth, and most
349 significantly, nutrient-specific effects could not be separated from growth rate-specific ones in (LIU *et al.*
350 2015). As we discussed earlier (see Figure 2), chemostats provide the only experimental approach for
351 properly studying how rates of cell proliferation may affect a given output, separately from any effects
352 unique to particular nutrients.

353 We observed a significant and disproportionate reduction of Cln3p-(Myc)₁₃ levels in slower-
354 proliferating cells (Figure 4A, B). With Cln3p-(Myc)₁₃ levels normalized against the total cellular protein
355 content, the fastest proliferating populations had >10-fold higher levels of Cln3p-(Myc)₁₃ compared to
356 the slowest proliferating cells (Figure 4A, B). Furthermore, because these estimates rely on the
357 hypermorphic *CLN3-13MYC* allele that produces a slightly stabilized Cln3p protein (THORBURN *et al.*
358 2013), the dynamic range of Cln3p levels as a function of doubling time is likely even broader.

359

360 **A uORF in *CLN3* adjusts the levels of Cln3p at different cell proliferation rates**

361 What is the mechanism that underpins the growth-dependent control of Cln3p abundance? We had
362 predicted that a uORF in *CLN3* could inhibit its translational efficiency in poor media disproportionately
363 (POLYMENIS AND SCHMIDT 1997). However, predictions of a growth-dependent role of the uORF had not
364 been accompanied with measurements of Cln3p levels. A kinetic model of protein synthesis (LODISH
365 1974) forecasts that removing the uORF would de-repress synthesis of Cln3p in slowly dividing cells
366 when the ribosome content of the cell is low. In contrast, removing the *CLN3* uORF would have minimal
367 effects in cells that proliferate fast, when the ribosome content is high. To test this model, we
368 introduced an A-315T substitution that mutates the start codon of the uORF in *CLN3* without affecting
369 *CLN3* mRNA levels (POLYMENIS AND SCHMIDT 1997), in the strain that expresses otherwise wild type Whi5p-
370 TAP and Cln3p-(Myc)₁₃ (see Materials and Methods). Note also that in chemostat conditions very similar

371 to the ones we used here, the levels of wild type *CLN3* mRNA do not change significantly as a function of
372 growth rate (BRAUER *et al.* 2008).

373 The effects of the uORF were evident in slower proliferating cultures ($T_d > 4h$), where the dynamic
374 range of Cln3p levels was much narrower (3-4 fold) in A-315T cells, and very different from the range of
375 Cln3p levels (10-fold) in their wild type counterparts at these longer doubling times ($p = 0.03648$, based
376 on the non-parametric Kolmogorov-Smirnov test), and indistinguishable from the range of Whi5p levels
377 (Figure 4A, B and File S1). We note that although the range of Cln3p levels is narrower in slower
378 proliferating *CLN3* uORF mutant cells (Figure 4), it is not flattened, arguing for additional mechanisms
379 that could adjust the levels of Cln3p at different growth rates. Nonetheless, an independent piece of
380 functional evidence further strengthened a growth-dependent role of the *CLN3* uORF. A hallmark
381 phenotypic readout of gain-of-function *CLN3* alleles is a reduction in cell size (NASH *et al.* 1988). Cells
382 that lack the *CLN3* uORF were smaller than their wild type counterparts were, and this effect was T_d -
383 dependent (see Figure 4C, D). Especially in leucine-limited cells, which displayed pronounced
384 enlargement as they proliferated slower, removing the *CLN3* uORF reduced their size substantially
385 (Figure 4D). These results are consistent with a de-repression of Cln3p synthesis upon removal of the
386 *CLN3* uORF.

387 These data argue that translational control contributes to the disproportionate reduction of Cln3p
388 levels as a function of T_d . Note also that loss of Cln3p severely perturbs the linear relation between T_d
389 and T_{G1} (Figures 3 and S3). In summary, our results underscore the critical role of the G1 cyclin Cln3p in
390 the physiological coupling between growth and division.

391 **DISCUSSION**

392 The scaling relations between G1 length and population time in yeast and human cells we report are
393 significant for several reasons. First, if the duration of G1 is estimated, they allow predictions of
394 proliferation rates, which could be useful in diverse settings, such as in tissues at an organismal level.
395 Second, they serve as benchmarks against which the effects of genetic or other perturbations can be
396 evaluated, as we demonstrated for Whi5p and Cln3p, two cell cycle regulators in yeast. Third, scaling
397 relations of cellular physiology may ultimately point to general, physical mechanisms that organize life at
398 the cellular level. In the next paragraphs, we discuss our findings in relation to current models of how
399 cell division is controlled by cellular biosynthetic capacity, with emphasis on the roles of Whi5p and
400 Cln3p.

401

402 **What is the context of this study in relation to others?**

403 Our results pertain to cell cycle kinetics of steady-state cultures that proliferate at different rates, not to
404 cell cycle adjustments immediately after nutrient shifts (TOKIWA *et al.* 1994; LEITAO AND KELLOGG 2017).
405 We also did not examine G1 progression in a particular cell cycle, where small daughter cells will not
406 initiate a new round of cell division until they reach a size characteristic of the culture medium
407 (HARTWELL AND UNGER 1977; JOHNSTON *et al.* 1977). Hence the scaling of G1 duration between populations
408 with different doubling times may not necessarily be controlled by the same mechanism that controls
409 how G1 duration is regulated to maintain size homeostasis within a population of cells that proliferates
410 at a given rate. This interpretation is consistent with the findings that cell size is not associated with
411 rates of cell proliferation (Figure 2), at least in experimental settings of steady-state chemostat cultures,
412 which separate nutrient-specific effects from the impact of different rates of cell proliferation. For
413 example, note the very different sizes of cells in glucose vs. leucine-limited cultures at the same dilution
414 rate (compare Figures 4C and 4D), offering yet another demonstration of how particular nutrients may

415 affect cell size independently of any changes in rates of cell proliferation. Furthermore, in leucine-
416 limited cultures, the cells were not only bigger than cells in glucose-limited chemostats at all dilution
417 rates tested, but they also got even bigger as they divided slower (Figure 4). These observations argue
418 against the widely-held assumptions that cells get smaller the slower they proliferate. Instead, they
419 support the notion that nutrient effects on cell size may be particular to specific nutrients, and not
420 associated with changes in rates of cell proliferation.

421

422 **How do our results mesh with models of G1 control?**

423 As we noted above, our data were from cells dividing at different rates, which was not addressed in the
424 Whi5p dilution model of (SCHMOLLER *et al.* 2015). Hence, the two studies are not directly comparable.
425 The Whi5p dilution model, however, was constructed on the basis that while Whi5p levels were
426 disproportionately lower than expected from cell growth, Cln3p levels were roughly constant and
427 proportional to the increase in size from birth to START (SCHMOLLER *et al.* 2015). Given the
428 disproportionate dependency of Cln3p levels on cell proliferation rates that we reported here and had
429 predicted earlier (POLYMENIS AND SCHMIDT 1997), could the uORF-mediated translational control of *CLN3*
430 affect Cln3p synthesis in the G1 phase from birth to START? We think this is unlikely because the uORF-
431 mediated translational control we described operates when the concentration of active ribosomes in
432 the cell changes (LODISH 1974), for example in poor vs. rich nutrients. Hence, while such translational
433 control mechanisms provide excellent conduits to disproportionately alter gene expression and
434 communicate growth-related inputs to downstream mRNA targets, to our knowledge, there is no report
435 of cell cycle-dependent changes in ribosome content. Other mechanisms, not due to changes in the
436 translational efficiency of *CLN3*, may contribute to significant, periodic changes in Cln3p abundance in
437 G1, within a given cell cycle.

438 There are conflicting reports in the literature about whether Cln3p ‘cycles’ in the cell cycle. Cln3p is
439 of such low abundance that cannot be properly measured in the single-cell microscopy methods of
440 (SCHMOLLER *et al.* 2015), because mutant *CLN3* alleles had to be used, producing extremely stabilized and
441 dysfunctional Cln3p protein that accumulates at very high, but non-physiological levels, so that it can be
442 visible with microscopy. The initial report claiming that Cln3p-HA levels were constant in the cell cycle
443 did not interrogate the early G1 phase (TYERS *et al.* 1993). In that report, although early G1, small (25 fL),
444 elutriated daughter cells were collected, Cln3p levels were not measured until much later in G1 (at 35 fL,
445 when by 40 fL 25% of the cells were already budded in that experiment; see Fig. 4 in (TYERS *et al.* 1993)).
446 Based on that result, it had been assumed for decades that Cln3p levels were constant in the cell cycle.
447 Recently, however, two independent studies by the Amon (THORBURN *et al.* 2013) and Kellogg (ZAPATA *et al.*
448 *et al.* 2014) labs, assayed elutriated synchronous cells carrying epitope-tagged, but otherwise wild type
449 *CLN3* alleles. Both studies showed that Cln3p levels change >10-fold in G1. Cln3p is absent in early G1
450 cells, while it rises dramatically before START. We also used the same *CLN3-13MYC* allele to monitor
451 Cln3p levels at different rates of cell proliferation (see Figure 4). The *CLN3-13MYC* allele is known to
452 produce a slightly stabilized Cln3p protein (THORBURN *et al.* 2013). Note that, on the face of the slight
453 stabilization of the Cln3p-(Myc)₁₃, the dynamic range of Cln3p levels as a function of growth rate we
454 report is likely even broader, not narrower. Hence, our conclusions are strengthened, not weakened by
455 the slight stabilization of the Cln3-Myc we used. For the same reasons, the changes in Cln3p levels in G1
456 observed previously (THORBURN *et al.* 2013; ZAPATA *et al.* 2014) are likely even greater than indicated in
457 these reports.

458 Overall, although a 2-fold dilution of Whi5p is observed in G1 (SCHMOLLER *et al.* 2015), the changes in
459 Cln3p levels are likely more pronounced (THORBURN *et al.* 2013; ZAPATA *et al.* 2014), through
460 transcriptional (ZAPATA *et al.* 2014), or other mechanisms. In this context, it is perhaps unsurprising that
461 we found Cln3p to be more important than Whi5p in the relation between T_d and T_{G1} . It is important to

462 stress, however, that any changes of Cln3p levels in G1 do not affect the key aspect of the inhibitor
463 dilution model, namely that Whi5p levels are reduced by cell growth. Hence, we may be dealing with a
464 more complex, 'mixed' model of inhibitor dilution *and* activator accumulation. It is possible that the
465 levels of additional proteins may behave analogously to Cln3p and Whi5p, contributing to a broader
466 network of factors whose antagonistic relations control the timing of initiation of cell division.
467 Regardless of the identity of those proteins, in yeast and other models, the fundamental relation
468 between T_{G1} and T_d we describe in this report will serve as a useful metric to evaluate the role of these
469 protein(s) in the control of cell division by growth inputs.

470 **ACKNOWLEDGEMENTS**

471 **Author Contributions:** Methodology, H.M.B., M.P.; Formal Analysis, H.M.B., M.P.; Investigation, H.M.B.,
472 M.C., I.P.E.P., A.O.P., M.P.; Resources, M.P.; Data Curation, H.M.B., M.P.; Writing – Original Draft, M.P.,
473 Writing – Review and Editing, H.M.B., M.P.; Visualization, H.M.B., M.P.; Supervision, H.M.B., M.P.,
474 Funding Acquisition, M.P.

475 This work was supported from the NIH (grant GM123139 to M.P.). M.C. was supported by a National
476 Science Foundation REU award (DBI-1358941). The authors declare no conflicts of interest.

477 **LITERATURE CITED**

- 478 Anastasia, S. D., D. L. Nguyen, V. Thai, M. Meloy, T. MacDonough *et al.*, 2012 A link between mitotic
479 entry and membrane growth suggests a novel model for cell size control. *J Cell Biol* 197: 89-104.
- 480 Aoki, Y., and G. E. Moore, 1970 Comparative study of mitotic stages of cells derived from human
481 peripheral blood. *Exp Cell Res* 59: 259-266.
- 482 Baserga, R., 1985 *The Biology of Cell Reproduction*.
- 483 Blank, H. M., R. Perez, C. He, N. Maitra, R. Metz *et al.*, 2017 Translational control of lipogenic enzymes in
484 the cell cycle of synchronous, growing yeast cells. *EMBO J* 36: 487-502.
- 485 Borenstein, M., 2009 *Introduction to meta-analysis*. John Wiley & Sons, Chichester, U.K.
- 486 Brauer, M. J., C. Huttenhower, E. M. Airoidi, R. Rosenstein, J. C. Matese *et al.*, 2008 Coordination of
487 growth rate, cell cycle, stress response, and metabolic activity in yeast. *Mol Biol Cell* 19: 352-
488 367.
- 489 Brons, P. P., J. M. Raemaekers, M. J. Bogman, P. E. van Erp, J. B. Boezeman *et al.*, 1992 Cell cycle kinetics
490 in malignant lymphoma studied with in vivo iododeoxyuridine administration, nuclear Ki-67
491 staining, and flow cytometry. *Blood* 80: 2336-2343.
- 492 Bryan, A. K., A. Engler, A. Gulati and S. R. Manalis, 2012 Continuous and long-term volume
493 measurements with a commercial Coulter counter. *PLoS One* 7: e29866.
- 494 Cerulus, B., A. M. New, K. Pougach and K. J. Verstrepen, 2016 Noise and Epigenetic Inheritance of Single-
495 Cell Division Times Influence Population Fitness. *Curr Biol* 26: 1138-1147.
- 496 Chan, Y. H., and W. F. Marshall, 2010 Scaling properties of cell and organelle size. *Organogenesis* 6: 88-
497 96.
- 498 Costanzo, M., J. L. Nishikawa, X. Tang, J. S. Millman, O. Schub *et al.*, 2004 CDK activity antagonizes Whi5,
499 an inhibitor of G1/S transcription in yeast. *Cell* 117: 899-913.
- 500 Cross, F. R., 1988 DAF1, a mutant gene affecting size control, pheromone arrest, and cell cycle kinetics of
501 *Saccharomyces cerevisiae*. *Mol Cell Biol* 8: 4675-4684.
- 502 de Bruin, R. A., W. H. McDonald, T. I. Kalashnikova, J. Yates, 3rd and C. Wittenberg, 2004 Cln3 activates
503 G1-specific transcription via phosphorylation of the SBF bound repressor Whi5. *Cell* 117: 887-
504 898.
- 505 Defendi, V., and L. A. Manson, 1963 Analysis of the life-cycle in mammalian cells. *Nature* 198: 359-361.
- 506 Di Talia, S., J. M. Skotheim, J. M. Bean, E. D. Siggia and F. R. Cross, 2007 The effects of molecular noise
507 and size control on variability in the budding yeast cell cycle. *Nature* 448: 947-951.
- 508 Dorsey, S., S. Tollis, J. Cheng, L. Black, S. Notley *et al.*, 2018 G1/S Transcription Factor Copy Number Is a
509 Growth-Dependent Determinant of Cell Cycle Commitment in Yeast. *Cell Syst* 6: 539-554.e511.
- 510 Dowling, M. R., A. Kan, S. Heinzl, J. H. Zhou, J. M. Marchingo *et al.*, 2014 Stretched cell cycle model for
511 proliferating lymphocytes. *Proc Natl Acad Sci U S A* 111: 6377-6382.
- 512 Elliott, S. G., and C. S. McLaughlin, 1978 Rate of macromolecular synthesis through the cell cycle of the
513 yeast *Saccharomyces cerevisiae*. *Proc Natl Acad Sci U S A* 75: 4384-4388.
- 514 Ferrezuelo, F., N. Colomina, A. Palmisano, E. Gari, C. Gallego *et al.*, 2012 The critical size is set at a single-
515 cell level by growth rate to attain homeostasis and adaptation. *Nat Commun* 3: 1012.
- 516 Fisher, R. P., 2016 Getting to S: CDK functions and targets on the path to cell-cycle commitment.
517 *F1000Research* 5: 2374.
- 518 Garmendia-Torres, C., O. Tassy, A. Matifas, N. Molina and G. Charvin, 2018 Multiple inputs ensure yeast
519 cell size homeostasis during cell cycle progression. *Elife* 7.
- 520 Garner, K. M., and A. Eastman, 2011 Variations in Mre11/Rad50/Nbs1 status and DNA damage-induced
521 S-phase arrest in the cell lines of the NCI60 panel. *BMC Cancer* 11: 206:201-213.

- 522 Guo, J., B. A. Bryan and M. Polymenis, 2004 Nutrient-specific effects in the coordination of cell growth
523 with cell division in continuous cultures of *Saccharomyces cerevisiae*. *Arch Microbiol* 182: 326-
524 330.
- 525 Hahn, A. T., J. T. Jones and T. Meyer, 2009 Quantitative analysis of cell cycle phase durations and PC12
526 differentiation using fluorescent biosensors. *Cell Cycle* 8: 1044-1052.
- 527 Hartwell, L. H., and M. W. Unger, 1977 Unequal division in *Saccharomyces cerevisiae* and its implications
528 for the control of cell division. *J Cell Biol* 75: 422-435.
- 529 Henry, K. A., H. M. Blank, S. A. Hoose and M. Polymenis, 2010 The unfolded protein response is not
530 necessary for the G1/S transition, but it is required for chromosome maintenance in
531 *Saccharomyces cerevisiae*. *PLoS One* 5: e12732.
- 532 Hoffman, J. G., 1949 Theory of the mitotic index and its application to tissue growth measurement. *Bull*
533 *Math Biophys* 11: 139-144.
- 534 Hoose, S. A., J. A. Rawlings, M. M. Kelly, M. C. Leitch, Q. O. Ababneh *et al.*, 2012 A systematic analysis of
535 cell cycle regulators in yeast reveals that most factors act independently of cell size to control
536 initiation of division. *PLoS Genet* 8: e1002590.
- 537 Hoose, S. A., J. T. Trinh, M. C. Leitch, M. M. Kelly, R. F. McCormick *et al.*, 2013 *Saccharomyces cerevisiae*
538 deletion strains with complex DNA content profiles. *FEMS Microbiol Lett* 345: 72-76.
- 539 Jagadish, M. N., and B. L. Carter, 1977 Genetic control of cell division in yeast cultured at different
540 growth rates. *Nature* 269: 145-147.
- 541 Johnston, G., R. Singer, S. Sharrow and M. Slater, 1980 Cell division in the yeast *Saccharomyces*
542 *cerevisiae* growing at different rates. *Microbiology* 118: 479-484.
- 543 Johnston, G. C., J. R. Pringle and L. H. Hartwell, 1977 Coordination of growth with cell division in the
544 yeast *Saccharomyces cerevisiae*. *Exp Cell Res* 105: 79-98.
- 545 Koch, A. L., 1966 The logarithm in biology. 1. Mechanisms generating the log-normal distribution exactly.
546 *J Theor Biol* 12: 276-290.
- 547 Koch, A. L., and M. Schaechter, 1962 A model for statistics of the cell division process. *J Gen Microbiol*
548 29: 435-454.
- 549 Kumei, Y., T. Nakajima, A. Sato, N. Kamata and S. Enomoto, 1989 Reduction of G1 phase duration and
550 enhancement of c-myc gene expression in HeLa cells at hypergravity. *Journal of Cell Science* 93:
551 221-226.
- 552 Leitao, R. M., and D. R. Kellogg, 2017 The duration of mitosis and daughter cell size are modulated by
553 nutrients in budding yeast. *The Journal of Cell Biology* 216: 3463-3470.
- 554 Lennartz, K. J., and W. Maurer, 1964 Autoradiographische Bestimmung der Dauer der DNS-Verdopplung
555 und der Generationszeit beim Ehrlich-Ascitestumor der Maus durch Doppelmarkierung mit 14C-
556 und 3H-Thymidin. *Zeitschrift für Zellforschung und Mikroskopische Anatomie* 63: 478-495.
- 557 Liu, X., X. Wang, X. Yang, S. Liu, L. Jiang *et al.*, 2015 Reliable cell cycle commitment in budding yeast is
558 ensured by signal integration. *Elife* 4.
- 559 Lodish, H. F., 1974 Model for the regulation of mRNA translation applied to haemoglobin synthesis.
560 *Nature* 251: 385-388.
- 561 Luciani, A. M., A. Rosi, P. Matarrese, G. Arancia, L. Guidoni *et al.*, 2001 Changes in cell volume and
562 internal sodium concentration in HeLa cells during exponential growth and following Isonidamide
563 treatment. *Eur J Cell Biol* 80: 187-195.
- 564 Mayhew, M. B., E. S. Iversen and A. J. Hartemink, 2017 Characterization of dependencies between
565 growth and division in budding yeast. *J R Soc Interface* 14.
- 566 Morgan, D. O., 2007 Control of Cell Proliferation and Growth, pp. 221 in *The Cell Cycle*. New Science
567 Press Ltd, London, UK.
- 568 Mosimann, J. E., Campbell, G., 1988 Applications in Biology: Simple Growth Models, pp. 287-302 in
569 *Lognormal distributions: theory and applications*

570 edited by E. Crow, L. Shimizu, K. Marcel, Dekker, Inc., New York.
571 Nash, R., G. Tokiwa, S. Anand, K. Erickson and A. B. Futcher, 1988 The WH1+ gene of *Saccharomyces*
572 *cerevisiae* tethers cell division to cell size and is a cyclin homolog. *EMBO J* 7: 4335-4346.
573 Palumbo, P., M. Vanoni, V. Cusimano, S. Busti, F. Marano *et al.*, 2016 Whi5 phosphorylation embedded
574 in the G1/S network dynamically controls critical cell size and cell fate. *Nat Commun* 7: 11372.
575 Pena, E. A., and E. H. Slate, 2006 Global Validation of Linear Model Assumptions. *J Am Stat Assoc* 101:
576 341.
577 Polymenis, M., 2017 Proteins associated with the doubling time of the NCI-60 cancer cell lines. *Cell*
578 *Division* 12: 6.
579 Polymenis, M., and E. V. Schmidt, 1997 Coupling of cell division to cell growth by translational control of
580 the G1 cyclin CLN3 in yeast. *Genes Dev* 11: 2522-2531.
581 Rivin, C. J., and W. L. Fangman, 1980 Cell cycle phase expansion in nitrogen-limited cultures of
582 *Saccharomyces cerevisiae*. *J Cell Biol* 85: 96-107.
583 Ross, D. T., U. Scherf, M. B. Eisen, C. M. Perou, C. Rees *et al.*, 2000 Systematic variation in gene
584 expression patterns in human cancer cell lines. *Nat Genet* 24: 227-235.
585 Scherf, U., D. T. Ross, M. Waltham, L. H. Smith, J. K. Lee *et al.*, 2000 A gene expression database for the
586 molecular pharmacology of cancer. *Nat Genet* 24: 236-244.
587 Schmoller, K. M., and J. M. Skotheim, 2015 The Biosynthetic Basis of Cell Size Control. *Trends Cell Biol*
588 25: 793-802.
589 Schmoller, K. M., J. J. Turner, M. Koivomagi and J. M. Skotheim, 2015 Dilution of the cell cycle inhibitor
590 Whi5 controls budding-yeast cell size. *Nature* 526: 268-272.
591 Siegel, A. F., 1982 Robust regression using repeated medians. *Biometrika* 69: 242-244.
592 Sisken, J. E., and R. Kinosita, 1961 TIMING OF DNA SYNTHESIS IN THE MITOTIC CYCLE IN VITRO. *J Biophys*
593 *Biochem Cytol* 9: 509-518.
594 Slater, M. L., S. O. Sharrow and J. J. Gart, 1977 Cell cycle of *Saccharomyces cerevisiae* in populations
595 growing at different rates. *Proc Natl Acad Sci U S A* 74: 3850-3854.
596 Soifer, I., and N. Barkai, 2014 Systematic identification of cell size regulators in budding yeast. *Molecular*
597 *systems biology* 10.
598 Soma, S., K. Yang, M. I. Morales and M. Polymenis, 2014 Multiple metabolic requirements for size
599 homeostasis and initiation of division in *Saccharomyces cerevisiae*. *Microb Cell* 1: 256-266.
600 Son, S., A. Tzur, Y. Weng, P. Jorgensen, J. Kim *et al.*, 2012 Direct observation of mammalian cell growth
601 and size regulation. *Nature methods* 9: 910-912.
602 Thorburn, R. R., C. Gonzalez, G. A. Brar, S. Christen, T. M. Carlile *et al.*, 2013 Aneuploid yeast strains
603 exhibit defects in cell growth and passage through START. *Mol Biol Cell* 24: 1274-1289.
604 Tokiwa, G., M. Tyers, T. Volpe and B. Futcher, 1994 Inhibition of G1 cyclin activity by the Ras/cAMP
605 pathway in yeast. *Nature* 371: 342-345.
606 Tyers, M., G. Tokiwa and B. Futcher, 1993 Comparison of the *Saccharomyces cerevisiae* G1 cyclins: Cln3
607 may be an upstream activator of Cln1, Cln2 and other cyclins. *Embo j* 12: 1955-1968.
608 Tyson, C. B., P. G. Lord and A. E. Wheals, 1979 Dependency of size of *Saccharomyces cerevisiae* cells on
609 growth rate. *J Bacteriol* 138: 92-98.
610 Tzur, A., R. Kafri, V. S. LeBleu, G. Lahav and M. W. Kirschner, 2009 Cell growth and size homeostasis in
611 proliferating animal cells. *Science* 325: 167-171.
612 Viechtbauer, W., 2010 Conducting meta-analyses in R with the metafor package. *J Stat Softw* 36: 1-48.
613 Zapata, J., N. Dephore, T. Macdonough, Y. Yu, E. J. Parnell *et al.*, 2014 PP2ARts1 is a master regulator of
614 pathways that control cell size. *J Cell Biol* 204: 359-376.

615

616 **FIGURE LEGENDS**

617 **Figure 1. Linking the length of the G1 phase with population doubling time.** Scatter plots of T_{G1} (**A, C**) or
618 T_{nonG1} (**B, D**) values on the x-axis, against T_d values (y-axis). All plots used the natural logarithms of the
619 values for yeast (**A, B**) and human (**C, D**) cells from Tables S1 and S2, respectively. The Kendall's (τ) rank
620 correlation coefficient is shown in each case. In red are regression lines of the Siegel repeated medians.
621 The slope and the associated 95% confidence intervals of the linear model are shown in each case.
622 Additional statistical parameters associated with these plots are shown in Table 1.

623 **Figure 2. Cell size does not correlate with T_d or T_{G1} in yeast.** Scatter plots of cell size values (x-axis)
624 against T_d (**A**) or T_{G1} (**D**) values (y-axis) from the data shown in Table S1. In red are regression lines of the
625 Siegel repeated medians. Forest plots of the measure of effect for each of the studies included in the
626 analysis (TYSON *et al.* 1979; GUO *et al.* 2004; BRAUER *et al.* 2008), based on the Kendall's (τ) rank
627 correlation coefficients (**B, E**), or Spearman's (r) rank correlation coefficients (**C, F**), are shown in each
628 case, for cell size vs. T_{G1} (**B, C**) and cell size vs. T_d (**E, F**). The confidence intervals from each study are
629 shown in parentheses and represented by horizontal whisker lines. In the studies in which the
630 confidence intervals overlap with the vertical line at the 0 point on the x-axis, their effect sizes do not
631 differ from no effect. The meta-analyzed measure of the effect is shown at the bottom of each plot,
632 based on random effects (RE) models.

633 **Figure 3. *Cln3p*, but not *Whi5p*, imposes the proper relation between T_{G1} and T_d .** Scatter plots of T_{G1}
634 values on the x-axis, against T_d values (y-axis). All plots used the natural logarithms of the values for wild
635 type (**A**) *whi5Δ* (**B**) or *cln3Δ* (**C**) cells, sampled from chemostat cultures several times at each dilution
636 rate, as indicated. For wild type and *whi5Δ* cells, in red are regression lines of the Siegel repeated
637 medians, and the slope of the linear models are shown (additional statistical parameters are in Table 1).
638 For *cln3Δ* cells, the red line shown simply connects the average values at each dilution rate. There is no

639 regression line because the relation between T_d and T_{G1} breaks down, especially at longer generation
640 times. Scatter plots of the relation of cell size and T_d in wild type (**D**) or cells lacking Whip5 (**E**) or Cln3p
641 (**F**), with cell size values (x-axis) plotted against T_d (y-axis) from the same cultures described in (**A-C**). All
642 the strains were in the BY4741 background (see Materials and Methods).

643 **Figure 4. The levels of the G1 cyclin Cln3p vary over a broad range as a function of T_d , due to a uORF**

644 **affecting translation of *CLN3*.** Scatter plots of the relative abundance (y-axis) of Cln3p-(Myc)₁₃ and

645 Whi5p-TAP in otherwise wild type *CLN3-13MYC*, *WHI5-TAP* cells (**A**), or *CLN3* uORF (*A-315T-CLN3*)

646 mutant cells (**B**), against T_d (x-axis). Each data point in the scatter plots is the average of immunoblot

647 signal intensities run in duplicate, and detected with antibodies against the Myc or TAP epitopes (see

648 Materials and Methods). All the raw immunoblots used to quantify protein levels are shown in the

649 Source Data (File S1). Before averaging, each individual signal intensity value was normalized against

650 loading in the corresponding immunoblot lane (visualized with Ponceau staining, see File S1 and

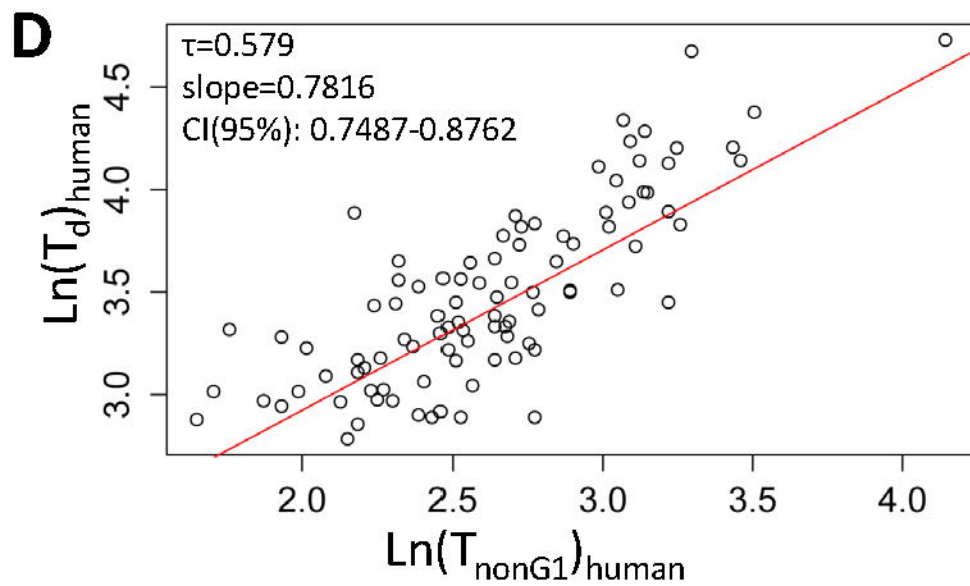
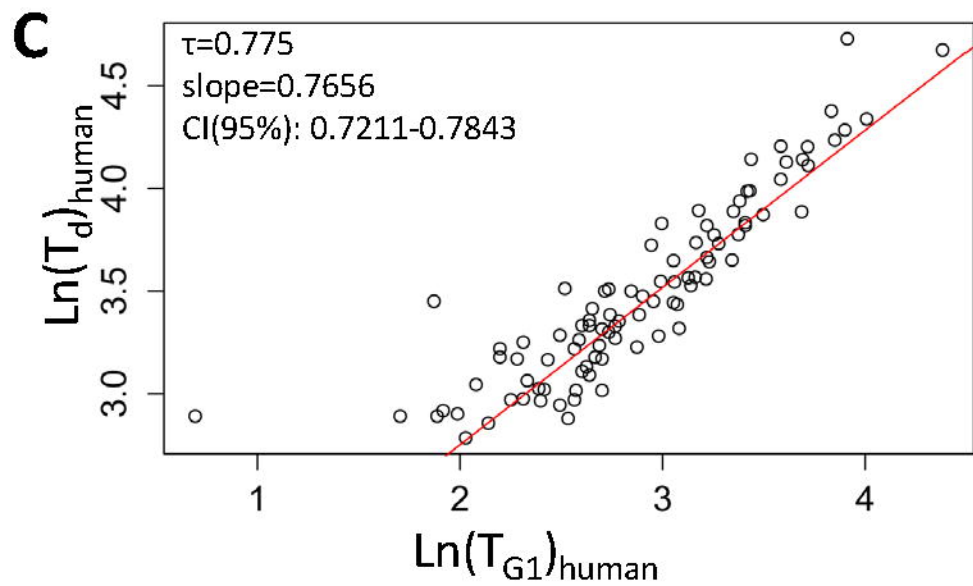
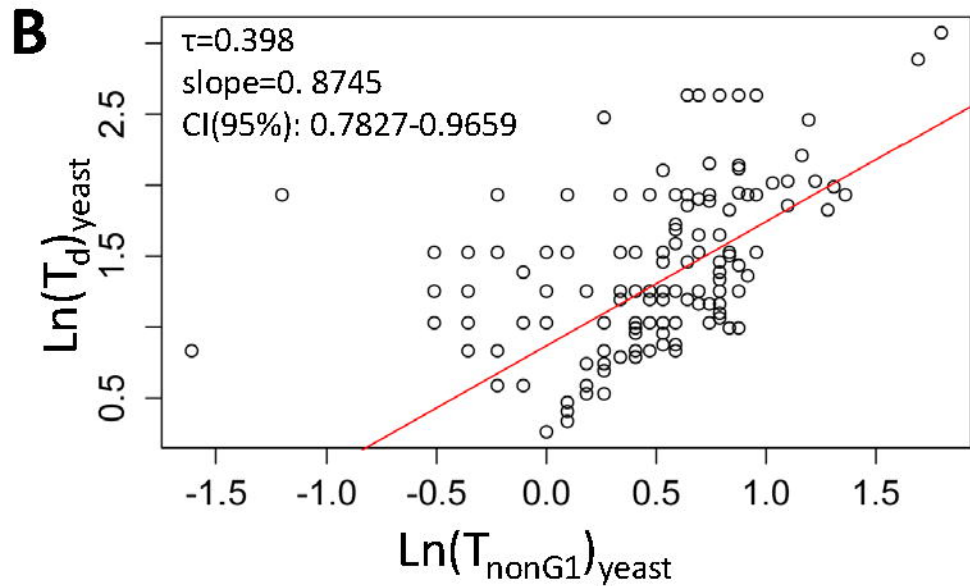
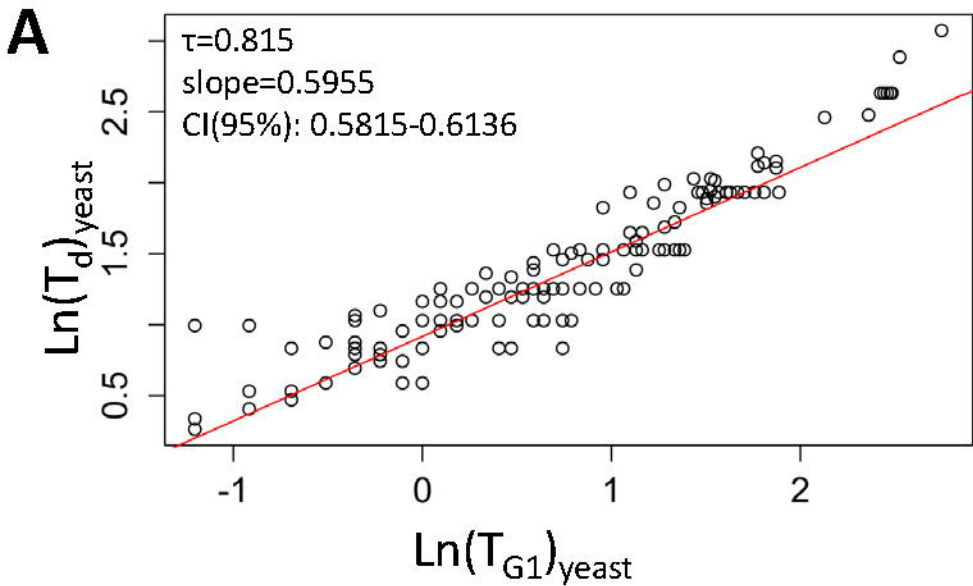
651 Materials and Methods). For each Cln3p-(Myc)₁₃ or Whi5p-TAP relative unit (r.u.) shown in the

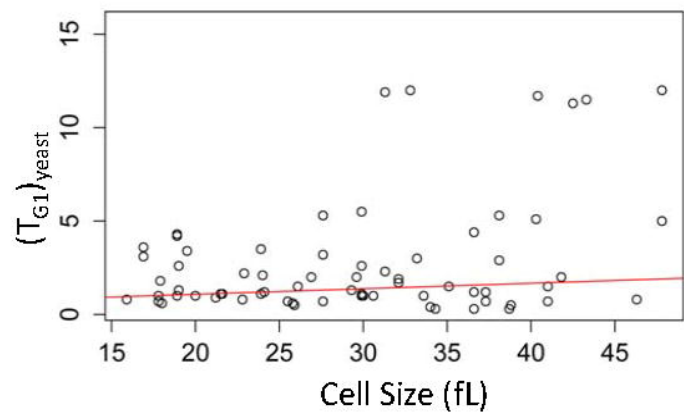
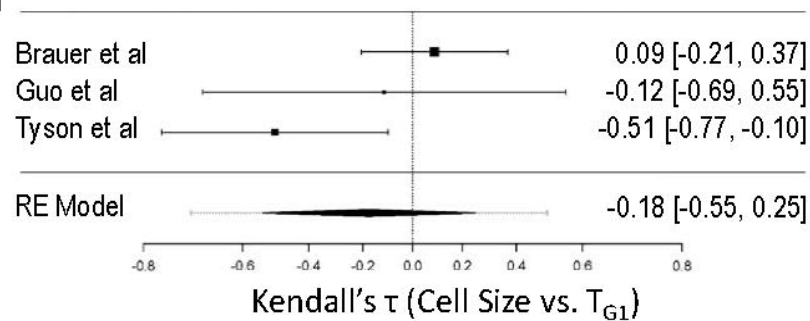
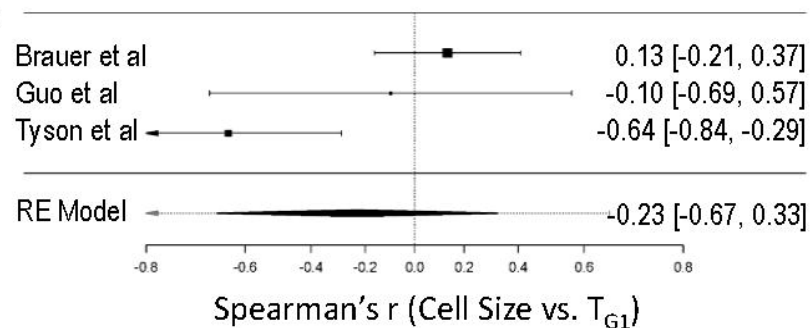
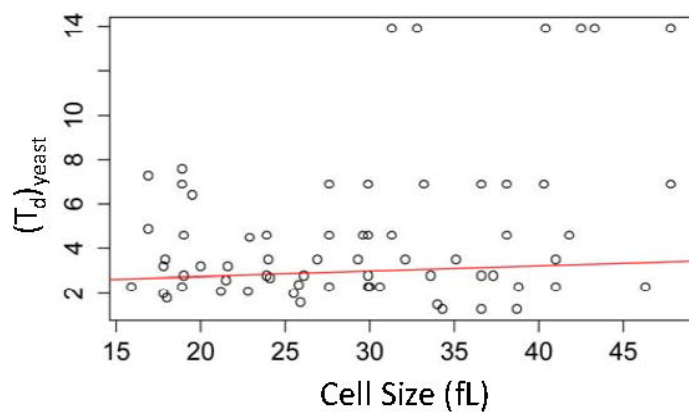
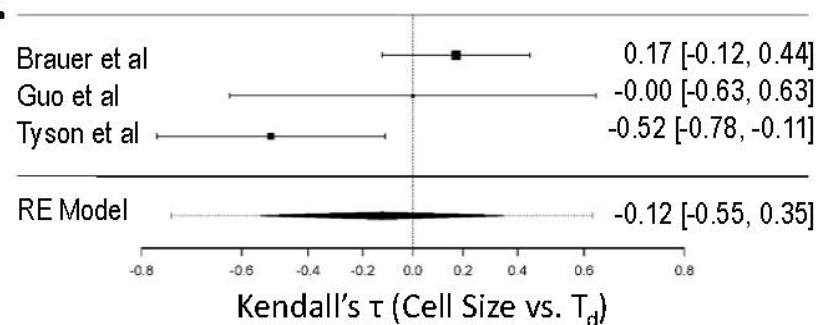
652 scatterplots (**A**, **B**), the normalized, averaged intensities were scaled by the lowest value (set to 1) for

653 each protein in the given chemostat experiment run at different dilution rates. Scatter plots of the

654 relation of cell size (x-axis) and T_d (y-axis) in the indicated strains, cultured under glucose (**C**) or leucine

655 (**D**) limitation, from the same cultures described in (**A**) and (**B**).



A**B****C****D****E****F**